10-2016

An Unexpected Restructuring of Combustion Soot Aggregates by Subnanometer Coatings of Polycyclic Aromatic Hydrocarbons

Chao Chen
New Jersey Institute of Technology

Xiaolong Fan
New Jersey Institute of Technology

Tasneem Shaltout
New Jersey Institute of Technology

Chong Qiu
University of New Haven, cqiu@newhaven.edu

Yan Ma
Nanjing University of Information Science and Technology

See next page for additional authors

Publisher Citation

Chen, C., X. Fan, T. Shaltout, C. Qiu, Y. Ma, A. Goldman, and A. F. Khalizov (2016), An unexpected restructuring of combustion soot aggregates by subnanometer coatings of polycyclic aromatic hydrocarbons, Geophys. Res. Lett. 43, 11,080–11,088, doi:10.1002/2016GL070877.

AGU PUBLICATIONS

Geophysical Research Letters

RESEARCH LETTER
10.1002/2016GL070877

Key Points:
- Solid PAH may form subcooled liquid films on the surface of soot particles at room temperature
- Subnanometer liquid-like films initiate significant restructuring of fractal soot aggregates
- PAH from incomplete fuel combustion may change particle morphology, altering aging pathways and atmospheric impacts of combustion aerosols

Supporting Information:
- Supporting Information S1

Correspondence to:
A. F. Khalizov,
khalizov@njit.edu

Citation:
Chen, C., X. Fan, T. Shaltout, C. Qiu, Y. Ma, A. Goldman, and A. F. Khalizov (2016), An unexpected restructuring of combustion soot aggregates by subnanometer coatings of polycyclic aromatic hydrocarbons, *Geophys. Res. Lett.*, *43*, 11,080–11,088, doi:10.1002/2016GL070877.

Received 30 AUG 2016
Accepted 15 OCT 2016
Accepted article online 19 OCT 2016
Published online 30 OCT 2016

An unexpected restructuring of combustion soot aggregates by subnanometer coatings of polycyclic aromatic hydrocarbons

Chao Chen[1,2], Xiaolong Fan[1,2], Tasneem Shaltout[1], Chong Qiu[3], Yan Ma[2], Andrew Goldman[4], and Alexei F. Khalizov[1]

[1]Department of Chemistry and Environmental Science, New Jersey Institute of Technology, Newark, New Jersey, USA, [2]Jiangsu Key Laboratory of Atmospheric Environment Monitoring and Pollution Control, Nanjing University of Information Science and Technology, Nanjing, China, [3]Department of Chemistry and Chemical Engineering, University of New Haven, New Haven, Connecticut, USA, [4]Livingston High School, Livingston, New Jersey, USA

Abstract We investigated the effect of thin polycyclic aromatic hydrocarbon (PAH) coatings on the structure of soot aggregates. Soot aerosol from an inverted diffusion burner was size classified, thermally denuded, coated with six different PAHs, and then characterized using scanning electron microscopy, light scattering, and mass-mobility measurements. Contrary to our expectation, significant restructuring was observed in the presence of subnanometer layers of pyrene, fluoranthene, and phenanthrene. These PAHs remained in subcooled liquid state in thin films, whereby the liquid layer acted as a lubricant, reducing the force required to initiate the restructuring. Thin layers of PAH of higher melting temperatures (perylene, anthracene, and triphenylene) presumably remained solid because these chemicals induced lesser structural changes. Our results suggest that some of the intrinsic PAH generated during incomplete combustion may induce significant restructuring of soot aggregates, even when present in small quantities, altering the properties and atmospheric impacts of combustion aerosols.

1. Introduction

Soot is a distinct type of carbonaceous material produced from incomplete combustion of carbonaceous fuels. Airborne soot particles are a major environmental pollutant, with negative impacts ranging from the reduction in air quality to climate warming [*Bond et al.*, 2013; *Shiraiwa et al.*, 2012]. The extent of these impacts depends strongly on the soot structure and composition, which vary significantly with the source and combustion regime [*Adachi and Buseck*, 2008; *Maricq*, 2007]. The mechanism of soot formation in combustion is highly complex and involves a large number of chemical and physical processes [*Kern and Xie*, 1991; *Mansurov*, 2005; *Richter and Howard*, 2000]. Under oxygen-deprived conditions, small radicals from fuel pyrolysis react to form acetylene, benzene, naphthalene, and larger polycyclic aromatic hydrocarbons (PAHs) [*Frenklach*, 2002; *Johansson et al.*, 2015; *Wang*, 2011]. When PAH concentration reaches a critical threshold, inception of small soot nuclei takes place, which then grow and lose hydrogen to form primary spherules (or monomers) consisting mostly of graphitic elemental carbon. The spherules coagulate through random collisions to produce loose aggregates with a fractal dimension of 1.8–2.1 [*Sorensen*, 2011]. Under certain combustion conditions, some of the PAH and aliphatic hydrocarbons generated in the flame can survive the combustion process [*Marr et al.*, 1999] and condense on soot aggregates, contributing from few percent to more than half of the particle mass [*Khalizov et al.*, 2012; *Sakurai et al.*, 2003; *Slowik et al.*, 2004].

The presence of intrinsic organic carbon on the surface of soot aggregates may significantly alter their environmental impacts and atmospheric aging pathways. For instance, PAHs show a broad spectrum of toxicity, including carcinogenicity and mutagenicity [*Shiraiwa et al.*, 2012]. Organic coatings can be attacked by atmospheric oxidants, such as the hydroxyl radical, ozone, and nitrogen dioxide [*Keyte et al.*, 2013], forming reactive oxygen species (ROS), which may cause significant damage to cell structures [*Ying et al.*, 2009]. If organic coatings are liquid, partitioning of semivolatile vapors may become possible in addition to condensation, significantly promoting the particle growth [*Pankow*, 1994]. Functionalization of the particle surface through oxidation, partitioning, and condensation increases soot hydrophilicity, transforming initially hydrophobic soot particles into cloud condensation nuclei (CCN) [*Ma et al.*, 2013b; *Zuberi et al.*, 2005] and ice nuclei [*Kulkarni et al.*, 2016]. Coated soot particles become more efficient light absorbers and even more efficient light scatterers [*Bond et al.*, 2006; *Khalizov et al.*, 2012; *Sorensen*, 2001].

The presence of coatings may induce significant irreversible changes in the structure of soot aggregates [*Bambha et al*., 2013; *Zhang et al*., 2008]. The extent of restructuring depends on the properties of the coating material and environmental conditions [*Ghazi and Olfert*, 2013]. Early studies have concluded that for liquid coatings, the force leading to compaction is the surface tension of the liquid that brings the primary spherules into a closer configuration to minimize the surface area and hence the surface energy [*Kütz and Schmidt-Ott*, 1992; *Mikhailov et al*., 1998]. Indeed, nonpolar liquids often cause less structural change [*Bueno et al*., 2011; *Slowik et al*., 2007] than polar liquids [*Khalizov et al*., 2009; *Saathoff et al*., 2003]. It has been suggested that unlike liquids, some solid coatings, such as anthracene and other PAHs, may anchor the spherules more firmly in place, protecting the backbone from access by liquid coatings and hence preventing rearrangement [*Slowik et al*., 2007]. A lack of restructuring during atmospheric aging may have significant implications to the evaluation of the impact of soot on climate because both experimental measurements [*Xue et al*., 2009] and calculations [*Scarnato et al*., 2013] indicate that the optical properties of soot depend on the aggregate compactness.

Accordingly, the initial goal of this study was to investigate the ability of intrinsic PAHs to anchor primary spheres in soot aggregates, preventing restructuring during subsequent atmospheric aging. Flame-generated soot aerosol was size classified, thermally denuded to remove traces of intrinsic organic carbon, and then recoated with selected PAHs. The coating fraction and morphology of soot aggregates were probed using mass-mobility measurements, scanning electron microscopy, and light scattering. Contrary to initial expectations, we discovered that several PAHs (pyrene, fluoranthene, and phenanthrene) induced a significant restructuring of soot aggregates even when present in the form of a subnanometer layer.

2. Experimental Methods

2.1. Soot Generation, Processing, and Mass-Mobility Analysis

Soot was generated through combustion of natural gas in an inverted diffusion-flame burner [*Coderre et al*., 2011; *Stipe et al*., 2005]. The burner produces a stable output of soot aerosol in a broad range of particle sizes and concentrations [*Kirchstetter and Novakov*, 2007]. Under most combustion conditions, the particles have no measurable organic material [*Ghazi et al*., 2013].

An integrated system (Figure S1 in the supporting information) consisting of two differential mobility analyzers (DMAs), an aerosol particle mass analyzer (APM), a condensation particle counter (CPC), two thermal denuders (TD), and a set of pickup chambers was used to process and characterize soot particles [*Gasparini et al*., 2004; *Khalizov et al*., 2009]. In some experiments, particles were collected on silicon chips (Ted Pella) using a custom-built electrostatic sampler [*Dixkens and Fissan*, 1999]. A more detailed description of the burner and aerosol system is provided in Text S1.

Mass-mobility measurements provided two primary parameters, particle mobility diameter (D) and particle mass (m), which were used to calculate several secondary parameters, including mobility diameter growth factor (Gfd), mass growth factor (Gfm), effective coating thickness (Δr), effective particle density (ρ), dynamic shape factor (χ), and mass-mobility scaling exponent (Dfm) [*DeCarlo et al*., 2004; *Khalizov et al*., 2013; *Sorensen*, 2011]. A detailed description of the derivation of these parameters and information on the repeatability of measurements is provided in Text S3.

2.2. SEM Analysis

Soot particles collected on silicon chips were imaged with a LEO 1530 VP Field Emission Scanning Electron Microscope (FESEM), using a 5 kV accelerating voltage. For each sample, 12 randomly selected individual particles were imaged at different magnifications. SEM micrographs were preprocessed using Adobe Photoshop to adjust contrast and/or levels and then by a suite of MATLAB-based codes to extract several particle parameters (Text S2) [*Dastanpour and Rogak*, 2014; *Soewono and Rogak*, 2011]. The parameters calculated from images include maximum projected length (L_{max}), maximum width (W_{max}), monomer area (A_p), total projected area of the aggregate (A_a), and perimeter of the particle (P). The average monomer diameter was calculated from individual aggregates by measuring 10–15 monomers in each aggregate. The compactness of aggregates was characterized using convexity and roundness (Figures S3 and S4). The convexity is the ratio of A_a over the area of the convex hull polygon, whereas the roundness represents

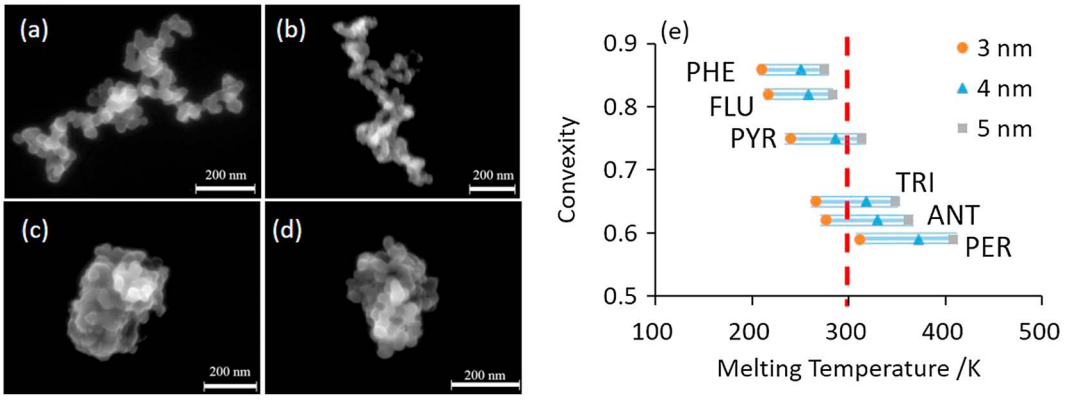

Figure 1. SEM imaging of soot aggregates (350 nm initial mobility diameter): (a) Fresh soot (b) coated with 0.92 nm ANT, (c) coated with 0.85 nm PHE, (d) coated with 0.85 nm PHE and then denuded, and (e) the dependence of convexity of coated aggregates on the PAH cluster melting temperature.

the elongation of the particle [*Chakrabarty et al.*, 2006; *China et al.*, 2015], as defined by equations (1) and (2), respectively,

$$\text{Convexity} = \frac{A_a}{A_{\text{polygon}}} \tag{1}$$

$$\text{Roundness} = \frac{4A_a}{\pi L_{\text{max}}^2} \tag{2}$$

The convexity and roundness vary between 0 and 1, the larger value representing more compact aggregates.

3. Results and Discussion

3.1. Morphological Changes in Soot Driven by PAH Layers

Figure 1a shows a typical SEM image of a 350 nm uncoated soot particle, which is an open aggregate of primary monomer spheres. The monomers vary in size (Figure S5), with an average diameter of 28 ± 7 nm, which is smaller than the monomer diameter produced by the inverted burner in previous studies (41 nm in *Coderre et al.* [2011] and 37 nm in *Ghazi and Olfert* [2013]) but larger than in the studies utilizing Santoro-style diffusion burner [*Khalizov et al.*, 2009; *Santoro et al.*, 1983]. The variation in the monomer size between studies is mainly caused by differing flame-quenching conditions, which depend on the global fuel equivalence ratio, flame temperature, and air/fuel flow speeds. In agreement with previous inverted burner studies [*Ghazi and Olfert*, 2013; *Ghazi et al.*, 2013], nascent soot aggregates contained less than 1% organic material by mass and exhibited a mass-mobility exponent of 2.22 (Table 2).

To investigate the anchoring effect of solid coatings, we exposed airborne soot aggregates to vapors of six different PAHs (Table 1), including anthracene (ANT), phenanthrene (PHE), pyrene (PYR), fluoranthene (FLU), triphenylene (TRI), and perylene (PER). All these PAHs are solids at room temperature, spanning a broad range of molecular weights, number and relative arrangement of aromatic rings, melting temperatures, and fusion enthalpies [*Roux et al.*, 2008; *Van Noort*, 2004]. Figure 1b shows the SEM image of a 350 nm soot aggregate coated with a 0.9 nm layer of ANT, as estimated from the particle mass measurement by the APM. The SEM resolution was insufficient to pinpoint the exact distribution of ANT on the aggregate surface. The coating may either evenly cover the aggregate or accumulate at junctions between primary spheres. Also, it is possible that during imaging some or all of the thin coating evaporated in high vacuum under the electron beam; for instance, particles composed of pure sulfuric acid or ammonium sulfate were stable at magnifications below about 15 k, but evaporated within seconds at magnifications above 200 k. Nevertheless, in agreement with our expectations, a thin layer of a solid ANT caused no visible impact on the structure of soot aggregates. Furthermore, soot aggregates that were first coated by ANT and then thermally denuded showed fractal morphology very similar to that of fresh and ANT-coated soot (Figure S6h).

When soot aggregates were coated with a comparable thickness layer of PHE, contrary to our expectations, significant structural changes were induced. As shown in Figure 1c, PHE-coated soot aggregates transformed

Table 1. Structure and Physical Properties of Studied PAH

Coating Material	Molecular Structure	Number of Rings	T_m [a]	T_{mc} [b]	$\Delta_{fus}H(T_m)$ [c]	T_b [d]	Density [e]	T_{chm} [f]
Phenanthrene (PHE)	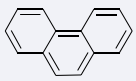	3	372	251	16.5	611	1.18	298–343 (328)
Anthracene (ANT)	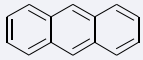	3	489	330	29.4	615	1.28	303–333
Pyrene (PYR)	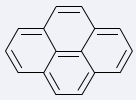	4	424	286	17.4	666	1.27	298–358 (343)
Triphenylene (TRI)	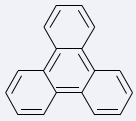	4	471	318	24.7	712	1.30	303–348
Fluoranthene (FLU)	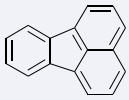	4	383	258	18.7	656	1.25	298–348 (318)
Perylene (PER)	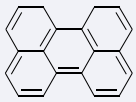	5	551	372	31.9	770	1.29	303–353

[a]Melting temperature, K.
[b]Cluster melting temperature, K (see discussion).
[c]Fusion enthalpy at melting temperature, kJ mol^{-1}.
[d]Boiling temperature, K.
[e]Material density, g cm^{-3}.
[f]Temperature of the pickup chamber wall, K; the values in parentheses correspond to the temperature of significant restructuring onset; the gas temperature at the chamber centerline typically was 2–10 K below the wall temperature.

to a more compact morphology when compared to nascent soot (Figure 1a) or ANT-coated soot (Figure 1b). Removal of the PHE coating through thermal denuding revealed a comparable compaction of the soot backbone as in the PHE-coated aggregate (Figure 1d). Having tested all six PAHs, we found that they fall into two distinct groups. The PAHs in the first group, including ANT, TRI, and PER, show a limited ability to restructure soot aggregates (Figures S6g, S6i, and S6k). The PAHs in the second group, including PHE, FLU, and PYR, can promote significant structural changes even when present in an amount corresponding to a subnanometer layer (Figures S6a, S6c, and S6e).

The extent of restructuring of coated soot aggregates can be gauged quantitatively using convexity and roundness derived from SEM images (Table 2). For nascent soot, these parameters were 0.43 ± 0.06 and 0.25 ± 0.08, respectively. In cases where no visual restructuring was observed, such as for soot coated with ANT, TRI, and PER, convexity and roundness increased to 0.55–0.65 and 0.29–0.36, respectively. For particles with obvious restructuring, i.e., those coated by PYR, FLU, and PHE, convexity increased to 0.75–0.88 and roundness increased to 0.45–0.66. No significant differences were observed between the convexity and roundness of coated and coated-denuded soot, indicating that restructuring preceded thermal denuding and was not caused, for instance, by heating of the coated aggregates in the TD.

To complement SEM imaging, mass-mobility measurements were carried out to characterize morphological changes in coated and coated-denuded soot aggregates. Figure 2 shows variations in Gfd, ρ_{eff}, χ, and Dfm in the 350 nm diameter soot aggregates that were coated by either PHE or ANT, or coated and then denuded

Table 2. Morphological Changes in Soot Aggregates After Processing Through PAH Coating and Thermal Denuding ($\Delta r = 0.84 \pm 0.12$ nm)

	Convexity [a]		Roundness [a]		Dfm [b]	
Coating Material	Coated	Coated/Denuded	Coated	Coated/Denuded	Coated	Coated/Denuded
No coating	0.43 ± 0.06		0.25 ± 0.08		2.22	
PAH With Higher Melting Temperature						
Perylene (PER)	0.60 ± 0.06	0.59 ± 0.07	0.29 ± 0.08	0.36 ± 0.09	2.31	2.19
Anthracene (ANT)	0.55 ± 0.11	0.62 ± 0.05	0.32 ± 0.12	0.31 ± 0.07	2.22	2.15
Triphenylene (TRI)	0.65 ± 0.09	0.65 ± 0.08	0.36 ± 0.08	0.42 ± 0.11	2.15	2.24
PAH With Lower Melting Temperature						
Pyrene (PYR)	0.75 ± 0.11	0.75 ± 0.13	0.45 ± 0.10	0.46 ± 0.14	2.57	2.68
Fluoranthene (FLU)	0.87 ± 0.05	0.82 ± 0.08	0.64 ± 0.13	0.59 ± 0.09	2.63	2.49
Phenanthrene (PHE)	0.88 ± 0.04	0.86 ± 0.08	0.66 ± 0.08	0.63 ± 0.13	2.62	2.74

[a] Convexity and roundness were derived from SEM images of deposited soot particles.
[b] Mass-mobility scaling exponent was derived from mass-mobility measurement of airborne soot particles.

(in latter case, Δr corresponds to the coating thickness before denuding). In Figure 2a, Gfd is plotted as a function of the relative change in the particle mass (Gfm) caused by the condensed PAHs, and also as a function of the associated effective coating thickness (Δr). For ANT, with the increase in Δr, there was a small (about 5% at $\Delta r = 0.8$ nm) increase in Gfd, while χ remained practically unchanged (Figure 2c), indicating that the coated aggregates maintained their highly irregular shape. Such behavior provides evidence that ANT was distributed uniformly over the aggregate rather than located at the junctions between monomers, because otherwise, a decrease in χ would have been observed. After thermal denuding, the soot backbone showed a small, less than 3% decrease in Gfd, confirming an insignificant restructuring by ANT. Accordingly, ρ_{eff} (Figure 2b) and Dfm (Figure 2d) remained practically unchanged. At a Δr of 0.75 nm, the effective densities of coated and coated-denuded soot were 0.27 and 0.31 g cm^{-3}, respectively. Compared with the 0.29 g cm^{-3} effective density of fresh soot, the change was less than 7%.

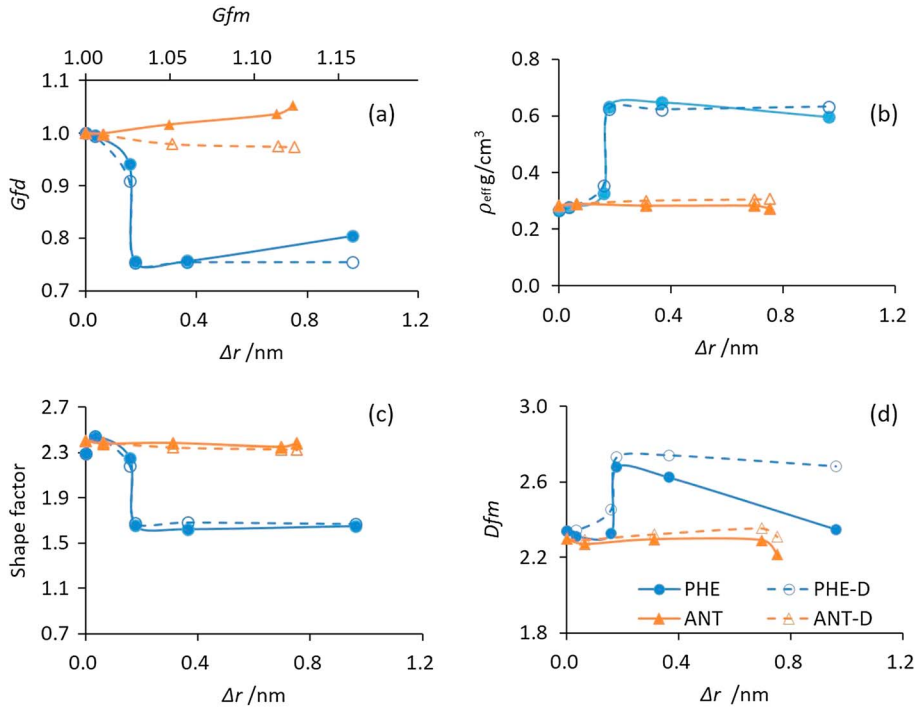

Figure 2. The effect of phenanthrene and anthracene coatings on morphology of soot aggregates as a function of the effective coating thickness (Δr): (a) Mobility diameter growth factor (Gfd), (b) effective density (ρ_{eff}), (c) dynamic shape factor (χ), and (d) mass-mobility exponent. Solid and dashed lines correspond to coated and coated-denuded soot, respectively.

In the case of PHE, there was an obvious decrease in Gfd already at the beginning of the coating process, followed by a steep drop when Δr approached a value of about 0.2 nm (Figure 2a). At this critical point, a maximum compaction was reached, beyond which the aggregate could not restructure any further. Figure 2b shows that the effective density more than doubled at the critical point as a result of compaction, increasing from 0.29 g cm^{-3} for fresh soot to 0.60 and 0.63 g cm^{-3} for coated and coated-denuded soot, respectively. The dynamic shape factor decreased from 2.43 to 1.65 for coated and 1.67 for coated-denuded soot, suggesting that the particles acquired less irregular shape as a result of exposure to the PHE coating layer. After the critical point, Gfd of coated particles started to rise with the increase in Δr. However, for coated-denuded soot aggregates, both Gfd and ρ_{eff} remained constant, confirming the above notion of complete compaction beyond the critical point.

Results of mass-mobility measurements for other particle sizes and other PAH coatings are provided in Text S3 and Figures S7–S10. Overall, FLU and PYR coatings behaved similarly to PHE, whereas TRI and PER behaved similarly to ANT, in agreement with SEM imaging results. The critical point depended on the initial size of soot aggregates and also on the properties of the coating material. The mass-mobility exponent remained practically unchanged for ANT but increased sharply at the critical point for PHE (Figure 2d). In the latter case, after the critical point Dfm remained nearly constant for coated-denuded soot, but showed an obvious decrease for coated soot, because for comparable pickup chamber temperatures, smaller particles gained relatively higher mass and also restructured less than larger particles. For this reason, Dfm of coated-denuded soot particles is a more reliable indicator of the structure of the aggregate backbone. As in previous reports, larger soot particles experienced a larger decrease in mobility diameter upon complete restructuring because they possessed more void space [*Pagels et al*., 2009]. The extent of restructuring also may have depended on the size of monomer spherules. In the study of *Ghazi and Olfert* [2013], who used oleic acid and dioctyl sebacate (DOS) coatings, at the critical point there was less than 15% size decrease for the 350 nm soot aggregates composed of 37 nm monomers, significantly less than the 25% decrease observed in our study for the aggregates composed of 28 nm monomers.

3.2. Restructuring Mechanism

Our experimental observation of soot restructuring by PAH is rather unexpected because these chemicals are all *solids* with relatively high melting temperatures (Table 1). The significant restructuring may indicate the presence of a subcooled *liquid-like* PAH layer on the aggregate surface. For liquid coatings, the restructuring is described qualitatively as a sequence of three interconnected events [*Glasstetter et al*., 1991; *Kütz and Schmidt-Ott*, 1992]. First, when a thin coat of a wetting liquid is formed on the aggregate surface, the molecules of the liquid replace the solid-solid contact by a solid-liquid contact in the meniscus between spherules, reducing the surface energy and enabling sliding and rolling of the monomers [*Kütz and Schmidt-Ott*, 1992]. The wettability depends on the liquid-solid material combination and generally is expected to be higher for liquids of a lower surface tension. Next, when menisci grow sufficiently large to overlap across several spherules, the force caused by the surface tension of the liquid brings the spherules into a closer configuration to minimize the surface energy further [*Khalizov et al*., 2009]. Liquids of higher surface tension are expected to promote restructuring more effectively at this stage. Finally, for the aggregate entirely immersed in a liquid droplet, if the liquid evaporates, the surface tension of the shrinking droplet may result in an additional compaction of the aggregate [*Ma et al*., 2013a].

Both theoretical and experimental studies indicate that a skin layer could remain liquid well below the melting temperature of solid bulk material, and in the case of small particles, a melting point depression scales inversely with the particle size [*Nanda*, 2009]. During the melting phase transition in pyrene and coronene clusters, nearly identical linear relationships have been observed between the reduced melting temperature (T_r) and reciprocal cluster size (d) for these two PAHs [*Chen et al*., 2014]. We used the relationship for pyrene ($T_r = 1 - 1.303/d$) to estimate the cluster melting temperature of the PAH in our study, assuming that the parameters derived for small clusters are applicable to thin films. The equivalent cluster diameter between 3 and 5 nm based on the range calculated by *Chen et al*. [2014] was chosen, which is well in excess of the effective coating thickness observed in our experiments (Figure 2). For all six PAHs there is a clear relationship between the aggregate convexity and coating T_{mc} (Figure 1e), where a lower convexity corresponds to more open aggregates coated by PAHs of a higher T_{mc}. Based on the estimated cluster melting temperatures, the PAHs fall into two groups (Figure 1e) with a boundary roughly corresponding to $d = 4$ nm (Table 1). The first

group, composed of PHE, PYR, and FLU, show a range of T_{mc} (251–286 K) that are all below ambient temperature. This finding is in accord with a study by *Aubin and Abbatt* [2006] who have suggested that adsorption of small PAHs on soot is described better using a subcooled liquid rather than a solid vapor pressure. As shown in Table 2, all three PAHs from the first group cause significant restructuring in soot aggregates. The second group (ANT, TRI, and PER) all have a T_{mc} (318–372 K) well above room temperature and these PAHs show lesser impact on the soot structure. Significant differences in the visual appearance of particles (Figure S6) and also sharply different mass-mobility profiles (Figure S7) further support this differentiation. In addition to lower bulk and cluster melting temperatures, the first group of PAHs show lower enthalpies of fusion (16.5–18.7 kJ mol^{-1}) than the second group (24.7–31.9 kJ mol^{-1}). It should be noted that other materials, such as glutaric (pentandioic) acid, also form subcooled liquid layers on the soot surface and promote the aggregate collapse [*Xue et al*., 2009].

The restructuring of soot in our experiments was caused by a *very thin* layer of PAH. Similar observations of soot restructuring by presumably subnanometer coating layers have been reported recently for oleic acid [*Bambha et al*., 2013] and several volatile organic liquids [*Miljevic et al*., 2012]. For restructuring to take place, the sliding and rolling of the monomers with respect to each other must be enabled. Although a subnanometer liquid layer may help loosen the connections between individual monomers, the presence of significantly thicker coatings is typically required to induce the collapse [*Ghazi and Olfert*, 2013; *Pagels et al*., 2009]. We ruled out that the PAH coating thickness could be significantly underestimated due to evaporative losses (Text S4). Furthermore, in experiments with well-studied coating materials, such as sulfuric acid and DOS, we confirmed that our soot aggregates had structural-mechanical properties comparable to those in previous studies (Text S5). Finally, using measurements of the enhancement in light scattering as an indicator of compaction (Text S6), we established that the air drag and electrostatic force play no role in restructuring. Thus, the restructuring is driven solely by the coating layer present on the aggregate rather than by forces external to the aggregate. Although our reported *effective* coating thickness is rather small, the coating material is not necessarily distributed uniformly over the aggregate surface. Even if uniformly condensed, initially, a liquid can flow toward small angle cavities between monomers to minimize the surface energy, if the coating layer is sufficiently thick [*Slowik et al*., 2007]. However, transport in thin layers, such as in our study, occurs on a timescale of hours [*Gao and Bhushan*, 1995; *Sedlacek et al*., 2015]. Thus, the condensation of PAH must have occurred preferentially into small angle cavities between monomers, driven by a significant depression of the equilibrium vapor pressure from the inverse Kelvin effect [*Crouzet and Marlow*, 1995]. Using a simple geometrical model, we estimated that a uniform coating layer with $\Delta r = 1$ nm is equivalent to ~10 nm thick pendular rings located at junctions between monomers. Such a ring thickness may be sufficient to provide forces required to initiate the aggregate collapse. One may assume that not all junctions are equal, some of them being less fused would be the first to yield in response to mechanical stress. The stress may be a result of the nonuniformly applied coating material, whereby the reduction in surface energy varies with position around a weak junction, causing mechanical failure and leading to restructuring.

4. Implications

Using mass-mobility measurements and SEM imaging, we show that significant structural changes can occur in soot aggregates coated by PAH. A very thin layer initiated an almost complete compaction in the case of phenanthrene, pyrene, and fluoranthene, but not in the case of anthracene, triphenylene, or perylene. The PAHs in the first group possess consistently lower melting temperatures; also, their extrapolated cluster melting temperatures T_{mc} are all below ambient, whereas T_{mc} of the second group are at least 20–70 K above ambient temperature. Based on these low values of T_{mc} together with our experimental findings of soot restructuring, we suggest that some of the PAHs produced during combustion may exist in liquid state on the particle surface. Since coatings on atmospheric soot may contain thousands of individual PAH [*Bouvier et al*., 2007; *Faccinetto et al*., 2011], further liquefaction through mixing becomes possible [*Peters et al*., 1997]. The presence of liquid films on solid particles may change their physical and chemical properties significantly. For instance, if the coating layer is liquid and can wet the soot surface, a significant restructuring may take place. The restructuring of soot aggregates can change their optical properties significantly, including both light scattering and light absorption. Additionally, the presence of liquid coatings can promote the partitioning of semivolatile vapors, enhancing the conversion of primary

aerosols to secondary aerosols. Accordingly, the impacts of aged primary particles on air quality and climate can be altered at a faster rate and to a greater extent [*Ma et al.*, 2013b].

Acknowledgments
This work was supported by the National Science Foundation (AGS 1463702 and 1463703). C.C. and X.F. acknowledge scholarships from the China Scholarship Council. T.S. acknowledges Provost Undergraduate Summer Scholarship from NJIT. The authors acknowledge the use of the SEM at the Otto H. York Center at NJIT and thank Shaima Parveen from the Livingston High School for her help with some of the experiments. Readers are referred to the supporting information for a complete set of data supporting the analysis and conclusions.

References

Adachi, K., and P. R. Buseck (2008), Internally mixed soot, sulfates, and organic matter in aerosol particles from Mexico City, *Atmos. Chem. Phys.*, *8*(21), 6469–6481.

Aubin, D. G., and J. P. Abbatt (2006), Laboratory measurements of thermodynamics of adsorption of small aromatic gases to n-hexane soot surfaces, *Environ. Sci. Technol.*, *40*(1), 179–187.

Bambha, R. P., M. A. Dansson, P. E. Schrader, and H. A. Michelsen (2013), Effects of volatile coatings and coating removal mechanisms on the morphology of graphitic soot, *Carbon*, *61*, 80–96.

Bond, T. C., G. Habib, and R. W. Bergstrom (2006), Limitations in the enhancement of visible light absorption due to mixing state, *J. Geophys. Res.*, *111*, D20211, doi:10.1029/2006JD007315.

Bond, T. C., et al. (2013), Bounding the role of black carbon in the climate system: A scientific assessment, *J. Geophys. Res. Atmos.*, *118*, 5380–5552, doi:10.1002/jgrd.50171.

Bouvier, Y., C. Mihesan, M. Ziskind, E. Therssen, C. Focsa, J. Pauwels, and P. Desgroux (2007), Molecular species adsorbed on soot particles issued from low sooting methane and acetylene laminar flames: A laser-based experiment, *Proc. Combust. Inst.*, *31*(1), 841–849.

Bueno, P. A., D. K. Havey, G. W. Mulholland, J. T. Hodges, K. A. Gillis, R. R. Dickerson, and M. R. Zachariah (2011), Photoacoustic measurements of amplification of the absorption cross section for coated soot aerosols, *Aerosol Sci. Technol.*, *45*(10), 1217–1230.

Chakrabarty, R. K., H. Moosmüller, W. P. Arnott, M. A. Garro, and J. Walker (2006), Structural and fractal properties of particles emitted from spark ignition engines, *Environ. Sci. Technol.*, *40*(21), 6647–6654.

Chen, D., T. S. Totton, J. W. Akroyd, S. Mosbach, and M. Kraft (2014), Size-dependent melting of polycyclic aromatic hydrocarbon nano-clusters: A molecular dynamics study, *Carbon*, *67*, 79–91.

China, S., G. Kulkarni, B. V. Scarnato, N. Sharma, M. Pekour, J. E. Shilling, J. Wilson, A. Zelenyuk, D. Chand, and S. Liu (2015), Morphology of diesel soot residuals from supercooled water droplets and ice crystals: Implications for optical properties, *Environ. Res. Lett.*, *10*(11), 114010.

Coderre, A., K. Thomson, D. Snelling, and M. Johnson (2011), Spectrally resolved light absorption properties of cooled soot from a methane flame, *Appl. Phys. B*, *104*(1), 175–188.

Crouzet, Y., and W. H. Marlow (1995), Calculations of the equilibrium vapor pressure of water over adhering 50–200-nm spheres, *Aerosol Sci. Technol.*, *22*(1), 43–59.

Dastanpour, R., and S. N. Rogak (2014), Observations of a correlation between primary particle and aggregate size for soot particles, *Aerosol Sci. Technol.*, *48*(10), 1043–1049.

DeCarlo, P. F., J. G. Slowik, D. R. Worsnop, P. Davidovits, and J. L. Jimenez (2004), Particle morphology and density characterization by combined mobility and aerodynamic diameter measurements. Part 1: Theory, *Aerosol Sci. Technol.*, *38*(12), 1185–1205.

Dixkens, J., and H. Fissan (1999), Development of an electrostatic precipitator for Off-line particle analysis, *Aerosol Sci. Technol.*, *30*(5), 438–453.

Faccinetto, A., P. Desgroux, M. Ziskind, E. Therssen, and C. Focsa (2011), High-sensitivity detection of polycyclic aromatic hydrocarbons adsorbed onto soot particles using laser desorption/laser ionization/time-of-flight mass spectrometry: An approach to studying the soot inception process in low-pressure flames, *Combust. Flame*, *158*(2), 227–239.

Frenklach, M. (2002), Reaction mechanism of soot formation in flames, *Phys. Chem. Chem. Phys.*, *4*(11), 2028–2037.

Gao, C., and B. Bhushan (1995), Tribological performance of magnetic thin-film glass disks: Its relation to surface roughness and lubricant structure and its thickness, *Wear*, *190*(1), 60–75.

Gasparini, R., R. J. Li, and D. R. Collins (2004), Integration of size distributions and size-resolved hygroscopicity measured during the Houston Supersite for compositional categorization of the aerosol, *Atmos. Environ.*, *38*(20), 3285–3303.

Ghazi, R., and J. Olfert (2013), Coating mass dependence of soot aggregate restructuring due to coatings of oleic acid and dioctyl sebacate, *Aerosol Sci. Technol.*, *47*(2), 192–200.

Ghazi, R., H. Tjong, A. Soewono, S. N. Rogak, and J. S. Olfert (2013), Mass, mobility, volatility, and morphology of soot particles generated by a McKenna and inverted burner, *Aerosol Sci. Technol.*, *47*(4), 395–405.

Glasstetter, R., C. I. Ricketts, and J. G. Wilhelm (1991), Towards modeling the meniscus geometry and volume of capillary water between two contacting microspheres in moist air, *J. Aerosol Sci.*, *22*(Suppl. 1), S195–S198.

Johansson, K. O., J. Y. W. Lai, S. A. Skeen, D. M. Popolan-Vaida, K. R. Wilson, N. Hansen, A. Violi, and H. A. Michelsen (2015), Soot precursor formation and limitations of the stabilomer grid, *Proc. Combust. Inst.*, *35*(2), 1819–1826.

Kern, R. D., and K. Xie (1991), Shock-tube studies of gas-phase reactions preceding the soot formation process, *Prog. Energy Combust. Sci.*, *17*(3), 191–210.

Keyte, I. J., R. M. Harrison, and G. Lammel (2013), Chemical reactivity and long-range transport potential of polycyclic aromatic hydrocarbons —A review, *Chem. Soc. Rev.*, *42*(24), 9333–9391.

Khalizov, A. F., R. Zhang, D. Zhang, H. Xue, J. Pagels, and P. H. McMurry (2009), Formation of highly hygroscopic soot aerosols upon internal mixing with sulfuric acid vapor, *J. Geophys. Res.*, *114*, D05208, doi:10.1029/2008JD010595.

Khalizov, A. F., B. Hogan, C. Qiu, E. L. Petersen, and R. Zhang (2012), Characterization of soot aerosol produced from combustion of propane in a shock tube, *Aerosol Sci. Technol.*, *46*(8), 925–936.

Khalizov, A. F., Y. Lin, C. Qiu, S. Guo, D. Collins, and R. Zhang (2013), Role of OH-initiated oxidation of isoprene in aging of combustion soot, *Environ. Sci. Technol.*, *47*(5), 2254–2263.

Kirchstetter, T. W., and T. Novakov (2007), Controlled generation of black carbon particles from a diffusion flame and applications in evaluating black carbon measurement methods, *Atmos. Environ.*, *41*(9), 1874–1888.

Kulkarni, G., et al. (2016), Ice nucleation activity of diesel soot particles at cirrus relevant temperature conditions: Effects of hydration, secondary organics coating, soot morphology, and coagulation, *Geophys. Res. Lett.*, *43*, 3580–3588, doi:10.1002/2016GL068707.

Kütz, S., and A. Schmidt-Ott (1992), Characterization of agglomerates by condensation-induced restructuring, *J. Aerosol Sci.*, *23*(Supplement 1), 357–360.

Ma, X., C. D. Zangmeister, J. Gigault, G. W. Mulholland, and M. R. Zachariah (2013a), Soot aggregate restructuring during water processing, *J. Aerosol Sci.*, *66*, 209–219.

Ma, Y., S. D. Brooks, G. Vidaurre, A. F. Khalizov, L. Wang, and R. Zhang (2013b), Rapid modification of cloud-nucleating ability of aerosols by biogenic emissions, *Geophys. Res. Lett.*, *40*, 6293–6297, doi:10.1002/2013GL057895.

Mansurov, Z. (2005), Soot formation in combustion processes (Review), *Combust., Explosion, Shock Waves*, *41*(6), 727–744.
Maricq, M. M. (2007), Chemical characterization of particulate emissions from diesel engines: A review, *J. Aerosol Sci.*, *38*(11), 1079–1118.
Marr, L. C., T. W. Kirchstetter, R. A. Harley, A. H. Miguel, S. V. Hering, and S. K. Hammond (1999), Characterization of polycyclic aromatic hydrocarbons in motor vehicle fuels and exhaust emissions, *Environ. Sci. Technol.*, *33*(18), 3091–3099.
Mikhailov, E. F., S. S. Vlasenko, A. A. Kiselev, and T. I. Ryshkevich (1998), Restructuring factors of soot particles, *Izvestiya - Atmos. Ocean Phys.*, *34*(3), 307–317.
Miljevic, B., N. C. Surawski, T. Bostrom, and Z. D. Ristovski (2012), Restructuring of carbonaceous particles upon exposure to organic and water vapours, *J. Aerosol Sci.*, *47*, 48–57.
Nanda, K. (2009), Size-dependent melting of nanoparticles: Hundred years of thermodynamic model, *Pramana*, *72*(4), 617–628.
Pagels, J., A. F. Khalizov, P. H. McMurry, and R. Y. Zhang (2009), Processing of soot by controlled sulphuric acid and water condensation—Mass and mobility relationship, *Aerosol Sci. Technol.*, *43*(7), 629–640.
Pankow, J. F. (1994), An absorption-model of the gas aerosol partitioning involved in the formation of secondary organic aerosol, *Atmos. Environ.*, *28*(2), 189–193.
Peters, C. A., S. Mukherji, C. D. Knightes, and W. J. Weber (1997), Phase stability of multicomponent NAPLs containing PAHs, *Environ. Sci. Technol.*, *31*(9), 2540–2546.
Richter, H., and J. B. Howard (2000), Formation of polycyclic aromatic hydrocarbons and their growth to soot—A review of chemical reaction pathways, *Prog. Energy Combust. Sci.*, *26*(4), 565–608.
Roux, M. V., M. Temprado, J. S. Chickos, and Y. Nagano (2008), Critically evaluated thermochemical properties of polycyclic aromatic hydrocarbons, *J. Phys. Chem. Ref. Data*, *37*(4), 1855–1996.
Saathoff, H., K. H. Naumann, M. Schnaiter, W. Schock, O. Mohler, U. Schurath, E. Weingartner, M. Gysel, and U. Baltensperger (2003), Coating of soot and (NH4)(2)SO4 particles by ozonolysis products of alpha-pinene, *J. Aerosol Sci.*, *34*(10), 1297–1321.
Sakurai, H., H. J. Tobias, K. Park, D. Zarling, S. Docherty, D. B. Kittelson, P. H. McMurry, and P. J. Ziemann (2003), On-line measurements of diesel nanoparticle composition and volatility, *Atmos. Environ.*, *37*(9–10), 1199–1210.
Santoro, R. J., H. G. Semerjian, and R. A. Dobbins (1983), Soot particle measurements in diffusion flames, *Combust. Flame*, *51*(2), 203–218.
Scarnato, B. V., S. Vahidinia, D. T. Richard, and T. W. Kirchstetter (2013), Effects of internal mixing and aggregate morphology on optical properties of black carbon using a discrete dipole approximation model, *Atmos. Chem. Phys.*, *13*(10), 5089–5101.
Sedlacek, A. J., E. R. Lewis, T. B. Onasch, A. T. Lambe, and P. Davidovits (2015), Investigation of refractory black carbon-containing particle morphologies using the single-particle soot photometer (SP2), *Aerosol Sci. Technol.*, *49*(10), 872–885.
Shiraiwa, M., K. Selzle, and U. Pöschl (2012), Hazardous components and health effects of atmospheric aerosol particles: Reactive oxygen species, soot, polycyclic aromatic compounds and allergenic proteins, *Free Radical Res.*, *46*(8), 927–939.
Slowik, J. G., K. Stainken, P. Davidovits, L. R. Williams, J. T. Jayne, C. E. Kolb, D. R. Worsnop, Y. Rudich, P. F. DeCarlo, and J. L. Jimenez (2004), Particle morphology and density characterization by combined mobility and aerodynamic diameter measurements. Part 2: Application to combustion-generated soot aerosols as a function of fuel equivalence ratio, *Aerosol Sci. Technol.*, *38*(12), 1206–1222.
Slowik, J. G., E. S. Cross, J. H. Han, J. Kolucki, P. Davidovits, L. R. Williams, T. B. Onasch, J. T. Jayne, C. E. Kolb, and D. R. Worsnop (2007), Measurements of morphology changes of fractal soot particles using coating and denuding experiments: Implications for optical absorption and atmospheric lifetime, *Aerosol Sci. Technol.*, *41*(8), 734–750.
Soewono, A., and S. Rogak (2011), Morphology and Raman spectra of engine-emitted particulates, *Aerosol Sci. Technol.*, *45*(10), 1206–1216.
Sorensen, C. (2011), The mobility of fractal aggregates: A review, *Aerosol Sci. Technol.*, *45*(7), 765–779.
Sorensen, C. M. (2001), Light scattering by fractal aggregates: A review, *Aerosol Sci. Technol.*, *35*(2), 648–687.
Stipe, C. B., B. S. Higgins, D. Lucas, C. P. Koshland, and R. F. Sawyer (2005), Inverted co-flow diffusion flame for producing soot, *Rev. Sci. Instrum.*, *76*(2), 023908.
Van Noort, P. C. (2004), Fugacity ratio estimations for high-melting rigid aromatic compounds, *Chemosphere*, *56*(1), 7–12.
Wang, H. (2011), Formation of nascent soot and other condensed-phase materials in flames, *Proc. Combust. Inst.*, *33*(1), 41–67.
Xue, H., A. F. Khalizov, L. Wang, J. Zheng, and R. Zhang (2009), Effects of coating of dicarboxylic acids on the mass-mobility relationship of soot particles, *Environ. Sci. Technol.*, *43*(8), 2787–2792.
Ying, Z. K., T. Kampfrath, G. Thurston, B. Farrar, M. Lippmann, A. X. Wang, Q. H. Sun, L. C. Chen, and S. Rajagopalan (2009), Ambient particulates alter vascular function through induction of reactive oxygen and nitrogen species, *Toxicol. Sci.*, *111*(1), 80–88.
Zhang, R., A. F. Khalizov, J. Pagels, D. Zhang, H. Xue, and P. H. McMurry (2008), Variability in morphology, hygroscopicity, and optical properties of soot aerosols during atmospheric processing, *Proc. Natl. Acad. Sci. U.S.A.*, *105*(30), 10,291–10,296.
Zuberi, B., K. S. Johnson, G. K. Aleks, L. T. Molina, and A. Laskin (2005), Hydrophilic properties of aged soot, *Geophys. Res. Lett.*, *32*, L01807, doi:10.1029/2004GL021496.